Journal of ELECTRONIC MATERIALS, Vol. 44, No. 4, 2015
DOI: 10.1007/s11664-014-3617-0

Structural Analysis and Dielectric Properties of $HoFe_{1-x}Ni_xO_3$ ($0 \leq x \leq 0.5$)

ZUBIDA HABIB,[1] KOWSAR MAJID,[1] M. IKRAM,[2,4] and K. ASOKAN[3]

1.—Department of Chemistry, National Institute of Technology, Hazratbal, Srinagar 190006, J&K, India. 2.—Department of Physics, National Institute of Technology, Hazratbal, Srinagar 190006, J&K, India. 3.—Materials Science Division, Inter University Accelerator Centre, New Delhi 110067, India. 4.—e-mail: ikram@nitsri.net

Bulk samples of $HoFe_{1-x}Ni_xO_3$ (x = 0, 0.1, 0.3, 0.5) were synthesized through the conventional solid-state reaction route and subjected to various structural and electrical characterization techniques. The x-ray diffraction patterns confirm that the samples exist in a single phase with orthorhombic structure having space group *Pbnm*. With increasing Ni content, the unit cell volume and lattice parameters undergo small variation, as further confirmed by Raman spectroscopy measurements, especially towards higher wavenumber. Dielectric loss and permittivity measurements were performed at varying temperature and frequency. The permittivity increases with Ni doping. Further, the permittivity and dielectric loss exhibited different behavior with temperature and frequency variation. The alternating-current conductivity results show a small-polaron-type contribution in the conduction mechanism of these orthoferrites.

Key words: Solid-state method, XRD, Raman, dielectric study, orthoferrites

INTRODUCTION

Ferrites have many applications in the modern world and are utilized in our daily life. The rare-earth-based orthoferrites, with chemical formula $RFeO_3$ (where R is a trivalent rare-earth ion), provide an opportunity to explore the mechanism of interaction between dissimilar magnetic ions: Fe–Fe, Fe–R, and R–R in decreasing order of strength. Further, it is observed that $RFeO_3$ materials are orthorhombically distorted perovskites with four formula units per unit cell, where Fe^{3+} lies on the orthorhombic site and R^{3+} on the twofold axis.[1–4] The perovskite structures form an important series of materials for magnetic studies and have been extensively studied since 1960 in both poly- and single-crystalline forms. Forestier et al. reported rare-earth orthoferrites and studied their magnetic properties. Magnetic and crystallographic measurements have been carried out on various members of the orthoferrite family.[5–14] These materials have opened new perspectives of scientific and technical interest in optomagnetic storage, logic events, and memory-based devices.[15,16] The promising magnetic, optical, and transport properties exhibited by these perovskite structures are due to the strong electron correlation effect in these systems. These observed novel phenomena lead to new concepts such as high-T_c superconductivity in cuprate systems, metal–insulator transitions, colossal magnetoresistance (CMR), and charge ordering in manganites.[17–20] These properties emerge due to the close interplay between magnetic and electronic properties arising from the simultaneous presence of strong electron–electron interaction potentials within the transition-metal *d*-orbitals and the sizable hopping interactions between the transition-metal *d*- and oxygen *p*-orbitals.[21–23]

The structural, magnetic, and electronic properties emerging on Ni doping of ferrites such as $LaFeO_3$ and $PrFeO_3$ result in semiconducting ferromagnetic behavior. It has been observed that Ni doping decreases the asymmetry in the hysteresis of magnetic structures and leads to structural distortions, insulator–metal transitions, and

(Received December 19, 2013; accepted December 31, 2014; published online February 11, 2015)

ferromagnetic to paramagnetic behavior. It also results in new magnetic behavior as well as spin reorientation in ferrites.[24,25] The chemical composition and synthesis process play an important role in enhancing the dielectric and magnetic properties of polycrystalline ferrites. Temperature, composition, and frequency are the principal parameters that determine the dielectric behavior, and the alternating-current (AC) electrical conductivity provides information about the type of conduction mechanism in ferrites based on the localized electric charge carriers.[26,27] Dielectric relaxation in ferroelectric capacitor structures has been shown to have substantial importance in applications, mostly in capacitors, memory integrated circuits (ICs), and sensors. Study of dielectric relaxation also provides unique information about the physical nature of the polarization, and the type and concentration of point defects.[28] Holmium (Ho) is a unique rare-earth metal due to its fascinating magnetic and dielectric properties. $HoFeO_3$ is a magnetic material having spontaneous magnetization as well as good dielectric properties.[29] The characteristic feature of $HoFeO_3$ is the presence of two magnetic subsystems, based on the rare-earth and iron ions, respectively.

The present study focuses on synthesis and characterization of $HoFeO_3$ and $HoFe_{1-x}Ni_xO_3$ (x = 0.1, 0.3, 0.5) with special reference to structural and dielectric properties. It is expected that Ni doping at Fe sites will change the structural, magnetic, and dielectric properties.

EXPERIMENTAL PROCEDURES

Polycrystalline bulk samples with chemical composition $HoFe_{1-x}Ni_xO_3$ (x = 0, 0.1, 0.3, 0.5) were synthesized through the solid-state reaction method. For heat treatment, a high-temperature chamber furnace (maximum temperature 1650°C/1700°C, working temperature 1600°C) was used. The temperature accuracy is ±2°C. The precursors Ho_2O_3, Fe_2O_3, and NiO (each of purity 99.9%) were weighed using a digital analytical balance according to the stoichiometric ratio after appropriate calculations. The weighed quantities of these desired powder samples were thoroughly and repeatedly ground in the presence of acetone (to improve homogeneity) using an agate mortar and pestle. The resultant powders were then precalcinated at 1000°C for 12 h and again ground and calcinated at 1200°C for 12 h. Finally, the samples were ground to fine powder (particle size 8.04 Å), pressed to pellet form (with diameter and thickness of 10 mm and 1 mm, respectively), and sintered at 1250°C for 24 h. To improve the homogeneity of the samples, this sintering procedure was repeated three times. The structure of the sample was analyzed by x-ray diffraction (XRD) using a Bruker D-8 Advance diffractometer (with Cu K_α radiation) at room temperature in the 2θ range from 20° to 80° with step size of 0.02°. Raman scattering measurements at room temperature, in the range of 200 cm^{-1} to 800 cm^{-1}, were performed using a Labram-HR800 micro Raman spectrometer equipped with a 50× objective, appropriate notch filter, and Peltier-cooled charge-coupled device detector. An Ar-ion laser with 514.5 nm wavelength was used for excitation of the Raman signals. The dielectric measurements of the prepared samples were carried out using an Agilent 4284A precision inductance–capacitance–resistance (LCR) meter as a function of the frequency of the applied alternating-current (AC) field in the range from 20 Hz to 1 MHz and at temperature ranging from 80 K to 400 K.

RESULTS AND DISCUSSION

Structural Analysis

The crystal structure of $HoFe_{1-x}Ni_xO_3$ (x = 0, 0.1, 0.3, 0.5) was analyzed by Rietveld refinement of the XRD profiles as recorded with a high-resolution diffractometer. The refined parameters included the cell dimensions, 2θ zero point, half-width, and background parameters. Figure 1a–d shows the XRD patterns of $HoFe_{1-x}Ni_xO_3$ (x = 0, 0.1, 0.3, 0.5) along with the fit curves and the difference line, clearly indicating that the XRD patterns are well fit by an orthorhombic structure with space group *Pbnm*. Bragg's *R*-factor for x = 0.0, 0.1, 0.3, and 0.5 was 12.3, 4.01, 7.83, and 56.7, respectively. The *RF*-factor for x = 0.0, 0.1, 0.3, and 0.5 was 8.15, 5.81, 6.49, and 17.6, respectively. From the XRD patterns of the samples, the lattice parameters and unit cell volume were calculated and are presented in Table I. It was observed that the lattice parameters showed a small variation with the Ni doping content. A similar trend was observed for the unit cell volume. This behavior indicates that Fe is being replaced by Ni, and may be attributed to the smaller ionic radius of Ni as compared with that of Fe. The small increase in lattice constants at x = 0.5 indicates that the orthorhombic structure is stable up to x = 0.3 whereas above this doping level some structural distortion takes place.

Raman scattering analysis allows determination of the fingerprint of the species present, being structure specific.[30] Raman spectra were recorded at room temperature as presented in Fig. 2. It was observed that the background in the spectra increased with the doping level. A similar effect was also seen as the doping concentration increased. It was established that these orthoferrites have an orthorhombically distorted perovskite structure with space group D_{2h} (*Pbnm*).[16] Group theory predicts the following phonon modes for this structure at the Brillouin zone center:[31,32]

$$7A_g + 5B_{1g} + 7B_{2g} + 5B_{3g} + 8A_u + 10B_{1u} + 8B_{2u} + 10B_{3u}.$$

The modes corresponding to the orthorhombic structure are A_g + B_{1g} symmetric and $2B_{2g}$ + $2B_{3g}$

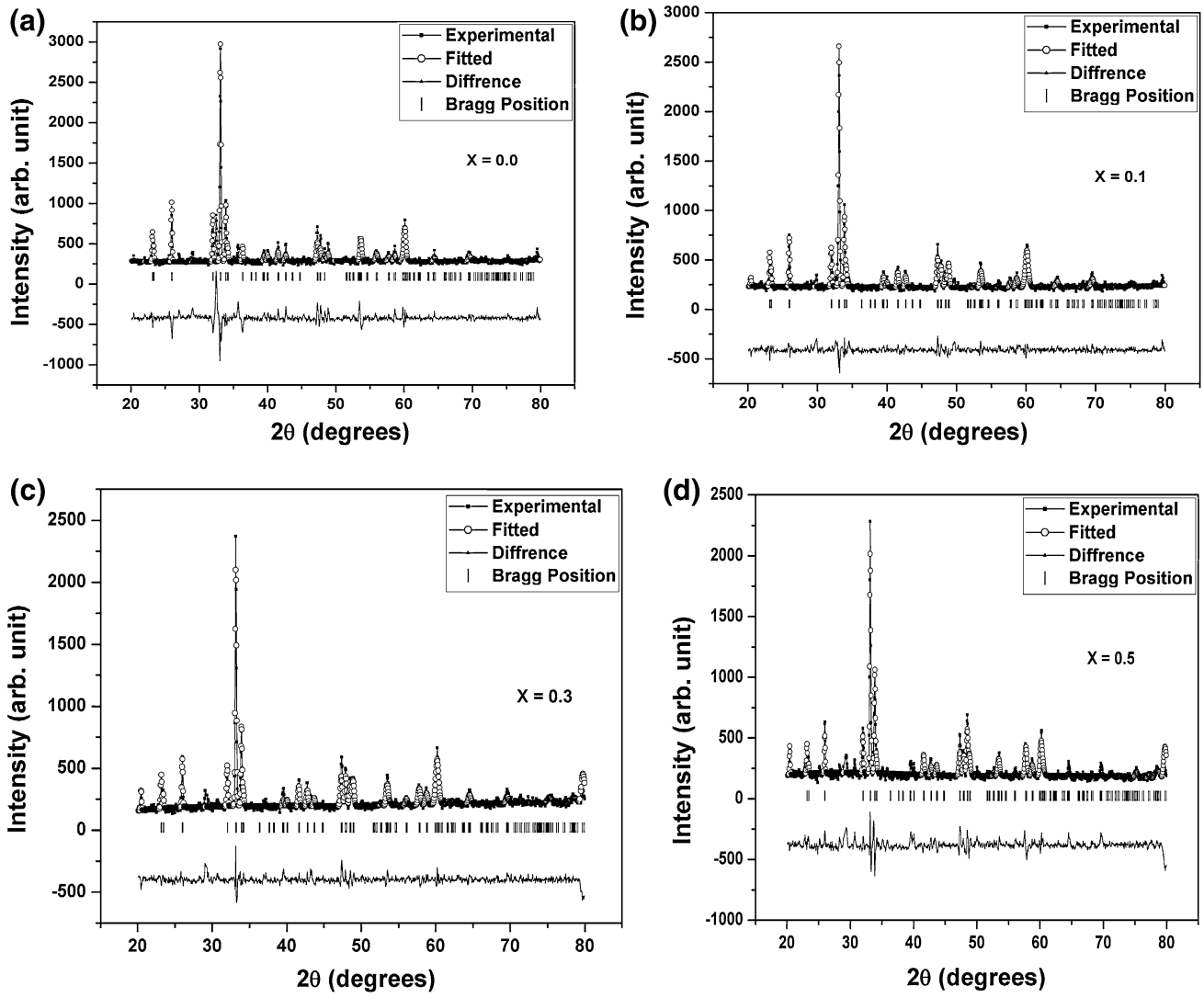

Fig. 1. XRD patterns of $HoFe_{1-x}Ni_xO_3$ with: (a) $x = 0.0$, (b) $x = 0.1$, (c) $x = 0.3$, and (d) $x = 0.5$.

Table I. Lattice parameters and unit cell volume for $HoFe_{1-x}Ni_xO_3$ ($x = 0, 0.1, 0.3, 0.5$)

Concentration (x)	Crystal Symmetry	a (Å)	b (Å)	c (Å)	Unit Cell Volume (Å)
0	Orthorhombic	5.284	5.590	7.609	224.752
0.1	Orthorhombic	5.282	5.588	7.605	224.436
0.3	Orthorhombic	5.281	5.586	7.594	224.036
0.5	Orthorhombic	5.288	5.602	7.599	225.140

antisymmetric stretching modes, $A_g + 2B_{1g} + B_{3g}$ bending modes, $2A_g + 2B_{2g} + B_{1g} + B_{3g}$ rotation, tilt modes of the octahedra, and $3A_g + B_{2g} + 3B_{1g} + B_{2g}$ modes related locally to rare-earth movements;[33] Of the $7A_g$ modes, two involve mainly motion of the rare-earth atom, two that of O(1), and three correspond to O(2). Of the $5B_{3g}$ modes, one corresponds to the rare-earth atom, one to O(1), and three to O(2). The iron atom participates only in infrared-active modes (being centrosymmetric).

The Raman spectra of Ni-doped $HoFeO_3$ at room temperature exhibit many modes, with high intensity at 495 cm^{-1}, 421 cm^{-1}, 339 cm^{-1}, and 266 cm^{-1}. Besides these modes, another mode at 629 cm^{-1} has the highest intensity. The Raman-active modes of $HoFeO_3$ were assigned as per Ref. 34 for $RFeO_3$ (R = Ho, Tb, Dy, Er, Tm) compounds. Most groups[35,36] have established that frequencies below 200 cm^{-1} are due to R^{3+} ions [external vibrations involving the motion of the

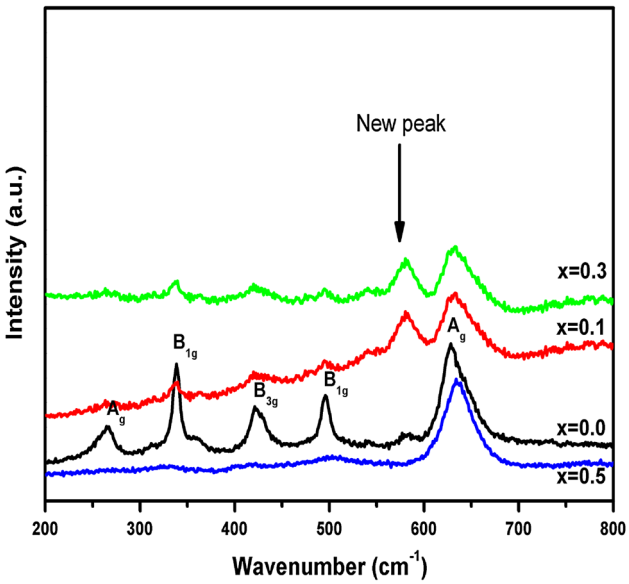

Fig. 2. Raman spectra of $HoFe_{1-x}Ni_xO_3$ (x = 0, 0.1, 0.3, 0.5).

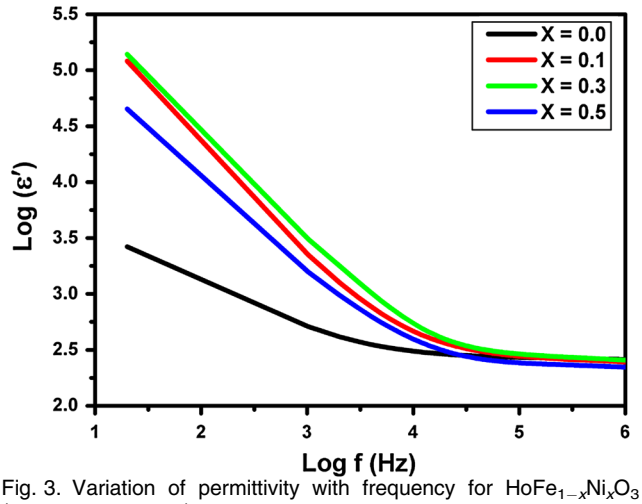

Fig. 3. Variation of permittivity with frequency for $HoFe_{1-x}Ni_xO_3$ (x = 0, 0.1, 0.3, 0.5) at room temperature.

rare-earth ion with respect to the Fe(or Ni)O_6 octahedra]. Further, the modes above 200 cm^{-1} are associated with oxygen ions. The high-wavenumber mode in the RFe(or Ni)O_3 crystal may be assigned to internal vibration related to mutual Fe(or Ni)–O motion within the oxygen octahedra. The frequency of oxygen-related modes is expected to increase if there is an increase in the R–O and Fe(or Ni)–O force constant, and hence bond length increases.[37] From Fig. 2 it is evident that, as the Ni content increases in $HoFe_{1-x}Ni_xO_3$ (x = 0.1, 0.3), a new peak starts to appear at around 582 cm^{-1}. The mode observed at 582 cm^{-1} corresponds to B_{3g} symmetry mode that arises due to antisymmetric stretching vibration of (Fe/Ni)O_6 octahedra. This mode is a silent mode in the orthorhombic structure, but appears after Ni doping of the system. This mode would be activated by the symmetry-breaking effects at the oxygen sites due to the replacement of Fe by Ni ions. A possible reason could be that Ni is smaller than Fe and the change in the bonding between oxygen and cations due to disorder/distortion induced in the system on doping. Further, the increase in the intensity of the mode at 582 cm^{-1} also indicates that the degree of disorder is increasing. At x = 0.5, the intensity of the Raman spectra decreases again, which is believed to be due to the disorder induced in the system by Ni doping. This is also supported by the XRD data. One of the most interesting characteristics of Raman scattering is its sensitivity to strain in the sample;[38] when the material is under strain, its Raman peak will shift from the original position or deform, enabling direct measurement of this mechanical quantity. It is well known that compressive stress results in shift of the position of the Raman peak towards higher cm^{-1} (commonly called "blue shift"), while tensile stress results in a shift towards lower cm^{-1} ("red shift").[39–41] In the present case, blue shift occurs after Ni doping in $HoFeO_3$, indicating compressive stress.

DIELECTRIC PROPERTIES

The dielectric constant in an AC field adopts the following complex form:

$$\varepsilon = \varepsilon' - j\varepsilon'', \tag{1}$$

where ε' is the real part and ε'' is the imaginary part, corresponding to the stored and dissipated energy, respectively. Figure 3 illustrates the frequency dependence of the real part of the permittivity of $HoFe_{1-x}Ni_xO_3$ (x = 0, 0.1, 0.3, 0.5) in an AC field with frequency ranging from 20 Hz to 1 MHz. These plots show a decrease in the permittivity at lower frequencies and steady behavior at higher frequencies. This behavior may be attributed to changes in valence states of cations and space-charge polarization resulting from creation of dipoles; the higher permittivity at lower frequencies is associated with heterogeneous conduction in these compounds.[42] The constant permittivity behavior at higher frequencies indicates the inability of the electric dipoles to follow the variation in the applied alternating electric field at such frequencies.[43]

From the Maxwell–Wagner model polaron hopping mechanism, it emerges that the electronic polarization contributes to low-frequency dispersion, which is in good agreement with the Koops model.[44–46] Hench et al. also reported the polarization mechanisms that occur at different frequencies that can be used to explain this type of dielectric behavior.[47] $HoFeO_3$ acquires very high permittivity at low frequency, consistent with the behavior of ferrites.[48,49] There are a large number of reports pertaining to abnormally high permittivity in certain ferrites.[50–52] Since the number of polarizable ions per unit volume is high due to the proximity of

oxygen ions in the close-packed structure, the polarization is enhanced on applying an electric field, leading to higher permittivity.

From Fig. 3 it is observed that the permittivity increases with increasing Ni content at any particular frequency. A possible explanation is related to

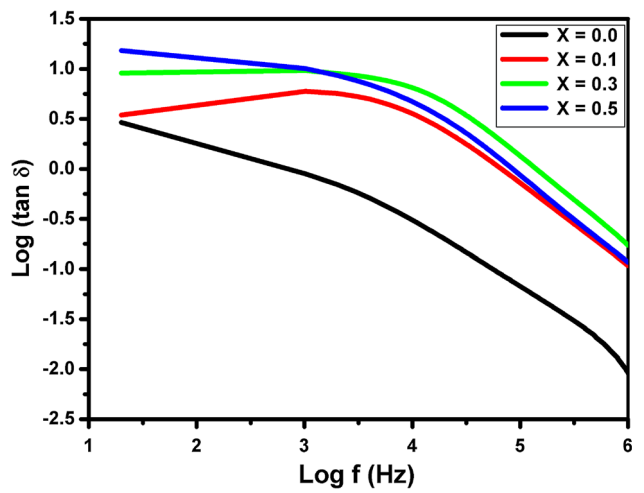

Fig. 4. Variation of dielectric loss with frequency for $HoFe_{1-x}Ni_xO_3$ (x = 0, 0.1, 0.3, 0.5) at room temperature.

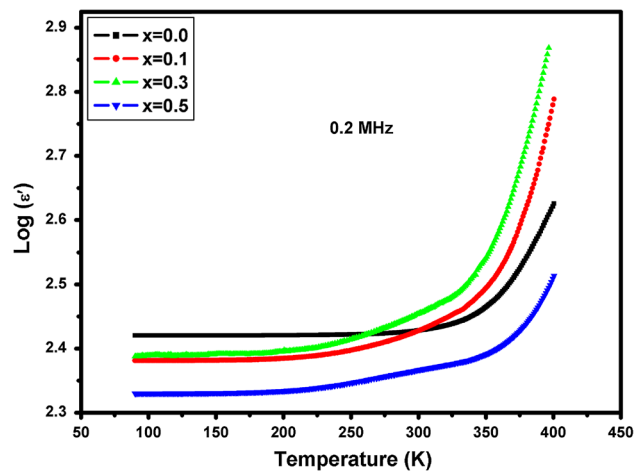

Fig. 6. Variation of permittivity with temperature at 0.2 MHz for $HoFe_{1-x}Ni_xO_3$ (x = 0, 0.1, 0.3, 0.5).

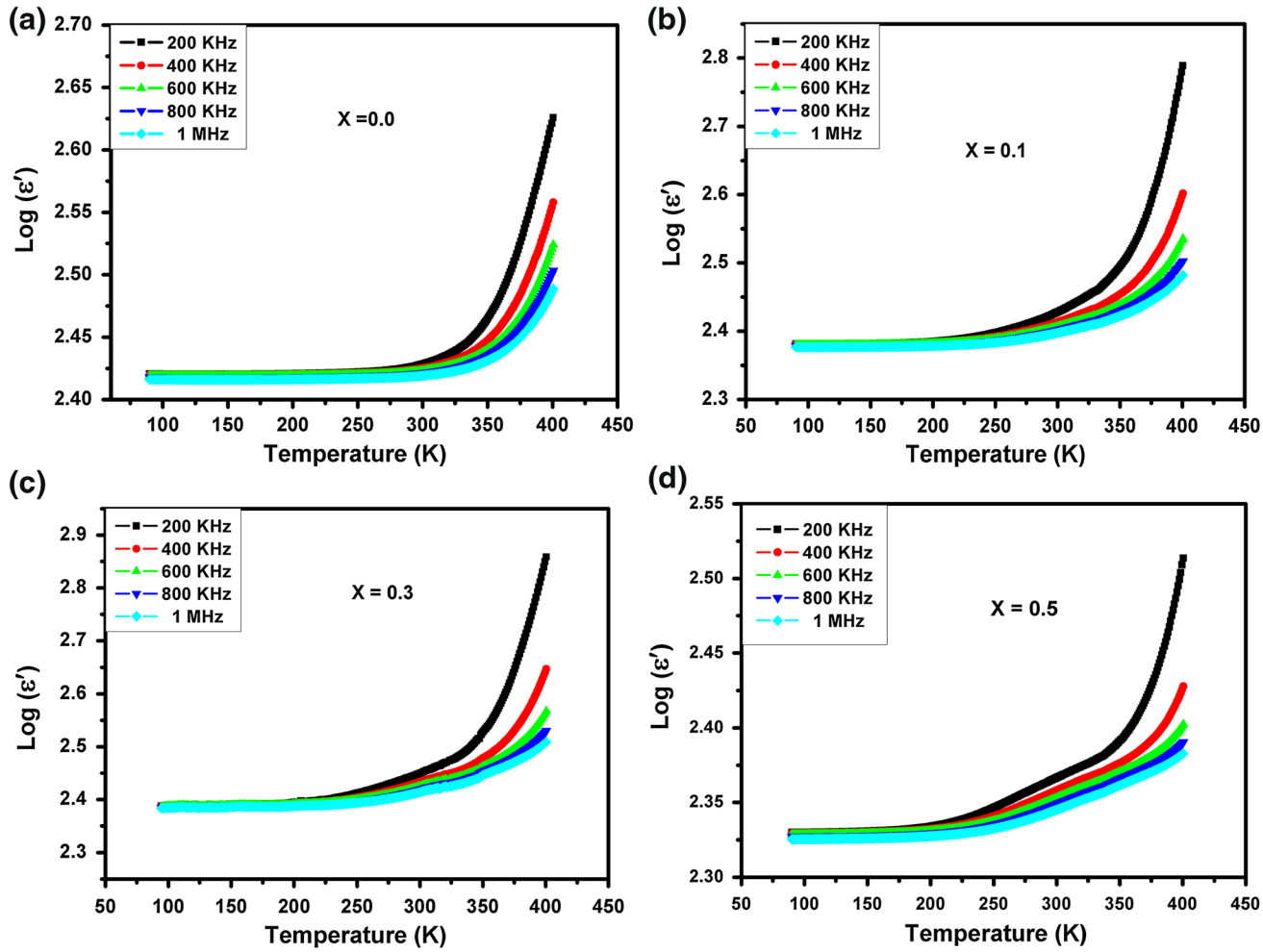

Fig. 5. Variation of permittivity with temperature at selected frequencies for $HoFe_{1-x}Ni_xO_3$ with: (a) x = 0.0, (b) x = 0.1, (c) x = 0.3, and (d) x = 0.5.

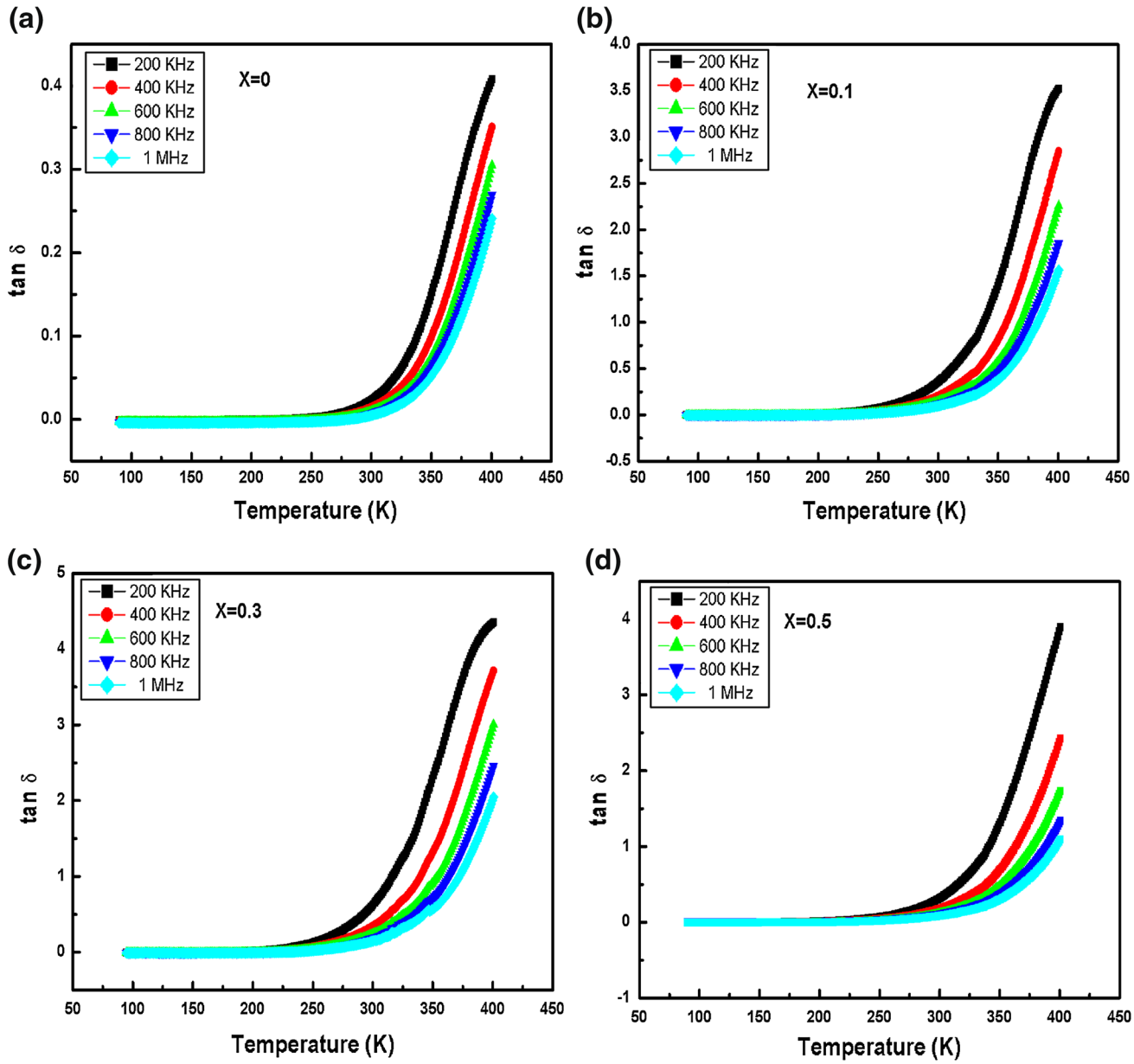

Fig. 7. Variation of dielectric loss with temperature at selected frequencies for $HoFe_{1-x}Ni_xO_3$ with: (a) $x = 0.0$, (b) $x = 0.1$, (c) $x = 0.3$, and (d) $x = 0.5$.

the B site in the perovskite ferrites, which plays a dominant role in the electrical conductivity phenomenon due to electron hopping on cations at B sites ($Fe^{3+} + e \leftrightarrow Fe^{2+}$). With Ni doping of $HoFeO_3$, chemical pressure is created in the compound and there is the possibility of either change of the Ni valence from divalent to trivalent state or reduction of the Fe valence from trivalent to divalent state to maintain charge neutrality. It thus follows that addition of Ni in place of Fe converts Fe^{3+} to Fe^{2+}, resulting in a decrease in the resistance of grains and thereby increasing the probability of electrons reaching the grain boundary. This is responsible for the increase in polarization and hence the permittivity.

The dielectric loss ($\tan \delta$) is a measure of the lag in the polarization with respect to the alternating field. The variation of the dielectric loss of $HoFe_{1-x}Ni_xO_3$ ($x = 0, 0.1, 0.3, 0.5$) as a function of frequency is shown in Fig. 4. It is evident that, for a particular dopant concentration, $\tan \delta$ decreases with increasing frequency and can be described using the Koops model. The low-frequency domain corresponds to higher resistivity, so acquisition of higher energy enhances the electron mobility between ions, resulting in greater energy loss. Similarly, there is a smaller energy loss in the higher-frequency region, which is due to the low resistivity.

The temperature dependence of the permittivity at selected frequencies for $HoFe_{1-x}Ni_xO_3$ ($x = 0, 0.1,$

0.3, 0.5) is shown in Fig. 5. The permittivity behaves independently of temperature at low temperature, while at higher temperature it increases with temperature for all frequencies; this behavior at higher temperature is due to the generation of extra thermal energy which enhances the mobility of charge carriers and hence increases the hopping rate, whereas the thermal energy at low temperature does not contribute to the mobility of charge carriers. This observed mechanism results in higher polarization at higher temperature, which increases the permittivity.

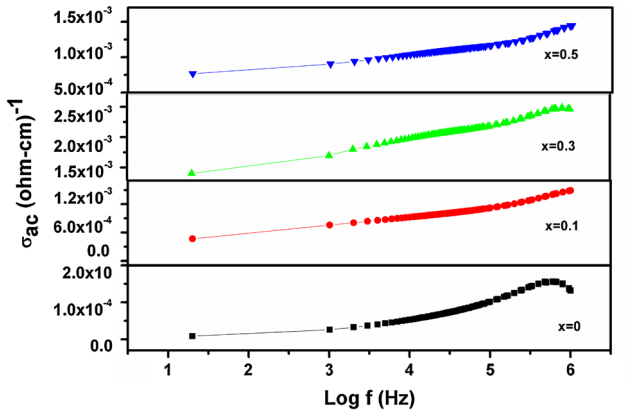

Fig. 8. Variation of AC conductivity with frequency for $HoFe_{1-x}Ni_xO_3$ (x = 0, 0.1, 0.3, 0.5) at room temperature.

The permittivity is a result of contributions from four types of polarization, namely interfacial, dipolar, ionic, and electronic.[53] The rapid increase in permittivity at lower frequency exhibits strong dependence on frequency and temperature and is caused by the interfacial and dipolar polarizations. The electronic and ionic polarizations are responsible for the permittivity developed at higher frequency, being independent of temperature; this indicates that the temperature dependence of the permittivity at higher frequencies is of little significance, resulting in low dispersion of the dielectric

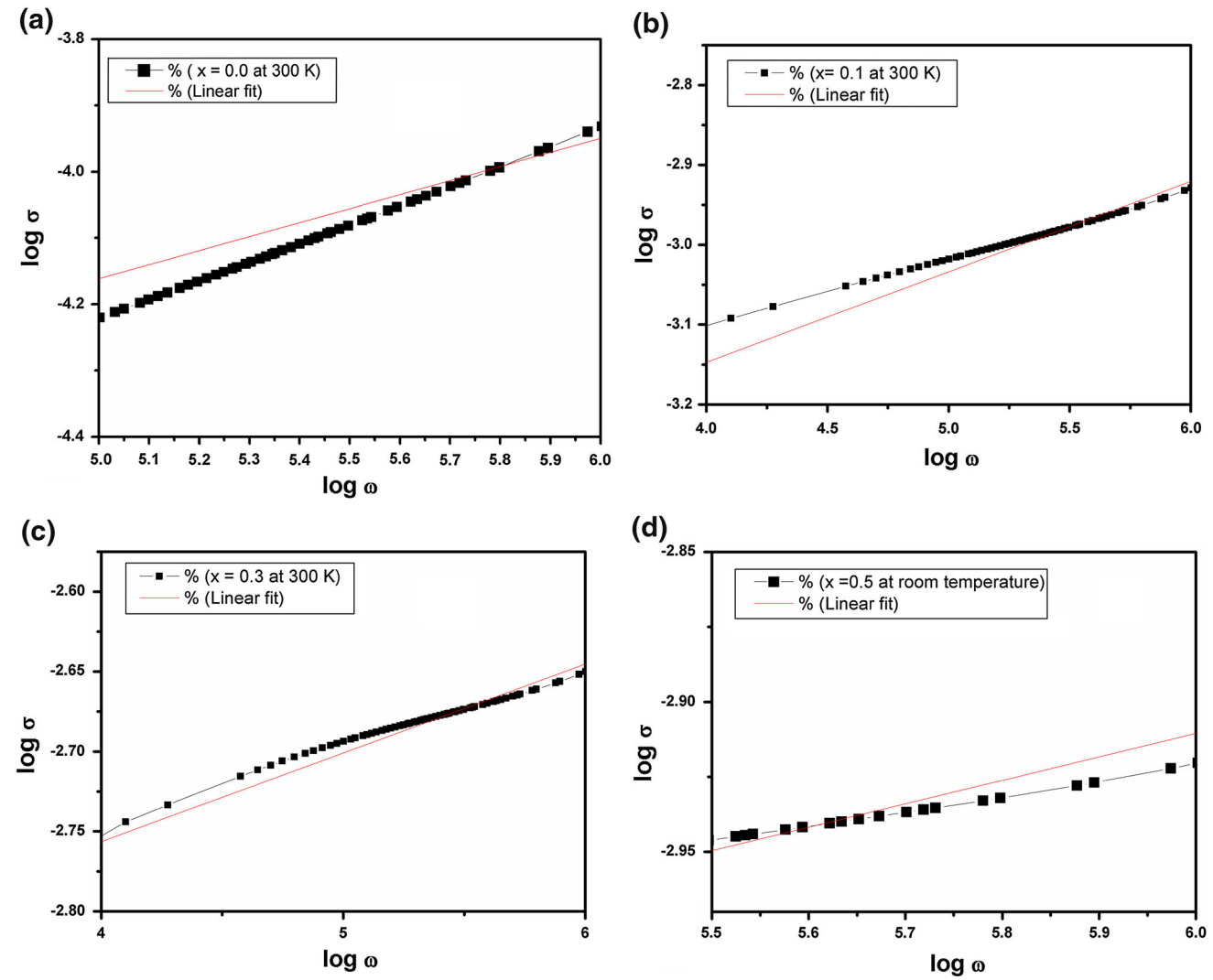

Fig. 9. log σ versus log ω for $HoFe_{1-x}Ni_xO_3$ with: (a) x = 0.0, (b) x = 0.1, (c) x = 0.3, and (d) x = 0.5.

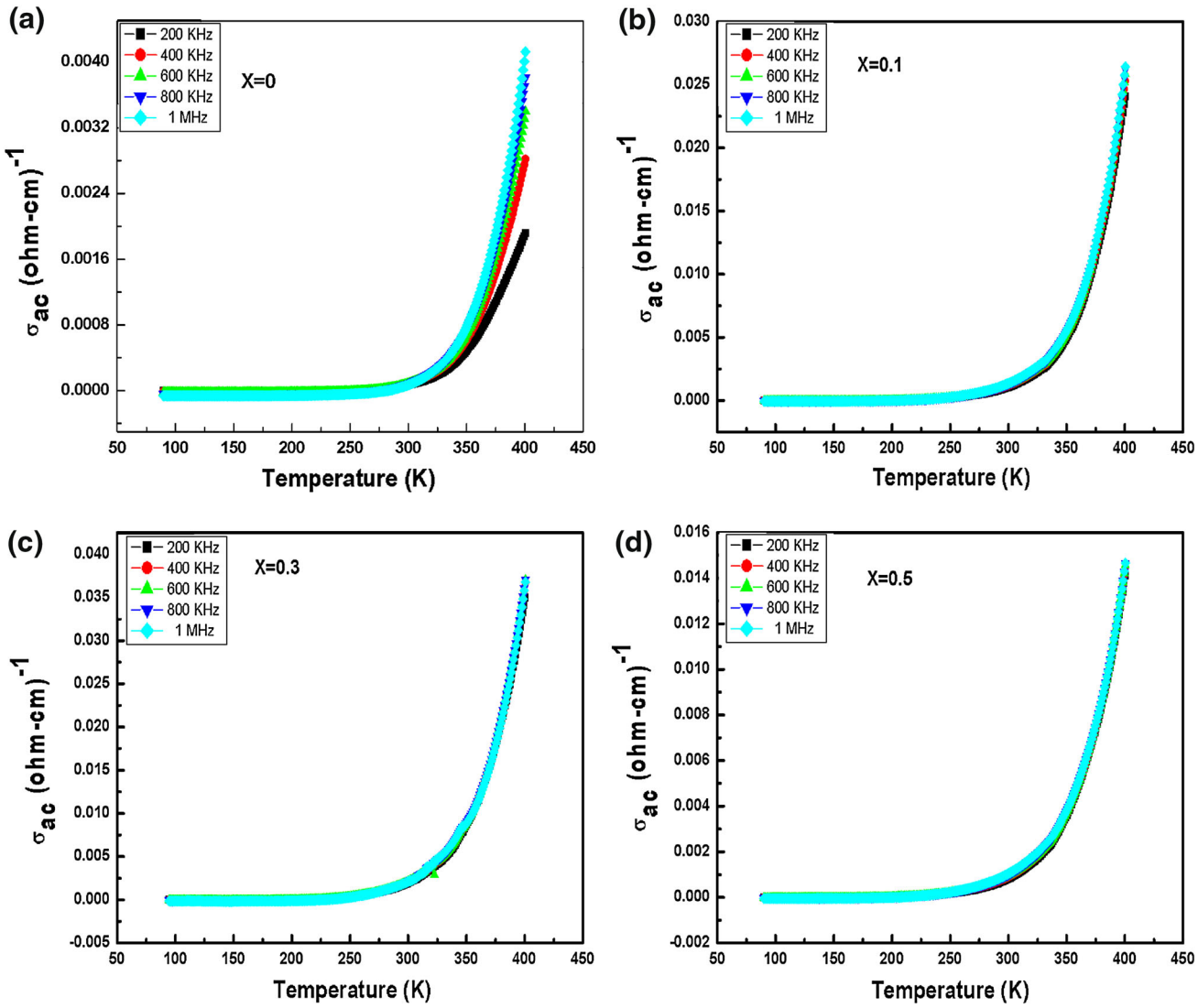

Fig. 10. Variation of AC conductivity with temperature at selected frequencies for $HoFe_{1-x}Ni_xO_3$ with: (a) $x = 0.0$, (b) $x = 0.1$, (c) $x = 0.3$, and (d) $x = 0.5$.

constant and thus explaining the temperature dependence of the permittivity at the various frequencies.

From Fig. 6, it is evident that the permittivity increases with Ni substitution at Fe sites in $HoFeO_3$ at given frequency and temperature. The temperature range for which the permittivity remains unaltered increases with increasing Ni doping concentration. Interestingly, we observed that, as a consequence of the Ni substitution, the main dielectric transition peak shifted towards higher temperature. A slight shift in peak position with increase in frequency depicts the presence of relaxor behavior in this system. The temperature dependence of the dielectric loss at selected frequencies is illustrated in Fig. 7. It is observed that this behavior is similar to that of the dielectric constant and can also be explained in a similar way as the case of permittivity. It is observed from these plots that the permittivity and dielectric loss decrease for higher Ni doping concentration ($x = 0.5$), which is due to structural change as evident from the XRD and Raman studies.

AC CONDUCTIVITY

The AC conductivity (σ_{AC}) was calculated using the following relation:

$$\sigma_{AC} = 2\pi f \varepsilon_0 \varepsilon' \tan\delta, \tag{2}$$

where $\varepsilon_0 = 8.854 \times 10^{-12}$ F m^{-1} and f is the frequency (in Hz) of the applied electric field. Figure 8 shows the variation of the AC conductivity with frequency at room temperature. Initially, the AC conductivity increases with frequency, but at higher frequencies the conductivity tends to decrease with further increase in frequency. A similar trend has been reported earlier.[54,55] The AC conductivity

provides evidence for whether the conduction mechanism corresponds to charge hopping between localized states or not. In the present case, the linearity of the plot indicates small-polaron-type conduction and is valid in ionic solids.[56] Such frequency dependence of the conduction attributable to small polarons has also been reported in the literature.[57] The hopping frequency of the charge carriers seems to depend on the frequency of the applied field and increases the mobility of the charge carriers. Since the conductivity is not increased by the number of charge carries but by their mobility, one expects the hopping of charge carriers to cease to follow the frequency of the applied field at a certain higher frequency, degrading the conductivity.

The AC conductivity for different doping concentrations at room temperature (300 K) as a function of frequency obeys Jonscher's power law and can be written as

$$\sigma_{\text{total}}(\omega) = \sigma_0 + A\omega^s, \tag{3}$$

where $\omega = 2\pi f$ is the measuring frequency, σ_0 is the direct-current (DC) conductivity corresponding to the frequency-independent plateau in the low-frequency region, and s is the power-law exponent. The power-law exponent s, which is a temperature-dependent quantity, lies between 0 and 1. A nonzero s value in the dispersive region of conductivity is due to energy stored in short-range collective motions of ions. A higher s values implies that greater energy is stored in such collective motions. The slope of the log σ versus log ω plots for the different compositions at room temperature in Fig. 9 directly provides the value of the power-law exponent s, which varies with the Ni doping concentration to 0.213, 0.113, 0.055, and 0.0783 for x = 0.0, 0.1, 0.3, and 0.5, respectively.

The AC conductivity with respect to temperature at particular frequencies for pristine ($HoFeO_3$) and doped samples is shown in Fig. 10. The AC conductivity shows a linear behavior with temperature for all frequencies, with a rapid increase at higher frequencies, which may be attributed to an increase in the number of charge carriers and their drift mobility when thermally activated. It is also observed from these plots that the AC conductivity decreases with higher Ni doping levels, which can again be attributed to the structural deformation caused at higher Ni concentration (x = 0.5).

CONCLUSIONS

Single-phase bulk samples of $HoFe_{1-x}Ni_xO_3$ (x = 0, 0.1, 0.3, 0.5) were synthesized by the solid-state reaction method, crystallizing in an orthorhombically distorted perovskite phase with space group *Pbnm*. Phase formation was confirmed by XRD and Raman spectroscopy. The unit cell volume decreases with the Ni concentration due to the difference in ionic radius between Fe and Ni ions. Substitution of Ni at Fe sites results in significant changes in the physical properties of $HoFeO_3$. Measurements of the permittivity, dielectric loss, and AC conductivity with frequency suggest that conduction in these materials is similar to other ferrites and occurs mainly due to polaron hopping. The low dielectric loss indicates that these materials are suitable for use in power applications at higher frequencies.

ACKNOWLEDGEMENTS

Financial support in the form of a fellowship from CSIR New Delhi to Z.H. is gratefully acknowledged. We thank IUAC, New Delhi for providing all experimental facilities.

REFERENCES

1. J.H. Park, T. Kimura, and Y. Tokura, *Phys. Rev. B* 58, R13330 (1998).
2. R.L. White, *J. Appl. Phys.* 4, 1061 (1969).
3. R.C. Le Craw, R. Wolfe, E.M. Gyorgy, F.B. Hagdorn, and J.C. Hensen, *J. Appl. Phys.* 39, 1019 (1968).
4. T. Yamaguchi, *J. Phys. Chem. Solids* 35, 479 (1974).
5. H. Forestier and G. Guit-Guillian, *Compt. Rend.* 230, 1884 (1950).
6. R.M. Bozorth, H.J. Williams, and D.E. Walsh, *Phys. Rev.* 103, 572 (1956).
7. R.M. Bozorth, V. Kramer, and J.P. Remeika, *Phys. Rev. Lett.* 1, 3 (1958).
8. S. Geller and E.A. Wood, *Acta Cryst.* 9, 563 (1956).
9. D. Treves, *Phys. Rev.* 125, 1843 (1962).
10. S. Geller, *J. Chem. Phys.* 24, 1236 (1956).
11. E.F. Bertaut, *Magnetism III*, ed. H. Suhl and G.T. Rado (New York: Academic, 1963), pp. 149–209.
12. D. Treves, *J. Appl. Phys.* 36, 1033 (1965).
13. G. Gorodetsky and D. Treves, *Proceedings of International Conference on Magnetism* (Nottingham, 1964), p. 606.
14. M. Eibschutz, *Acta Cryst.* 19, 337 (1965).
15. H.R. Karp, *Electronics* 42, 83 (1969).
16. U. Raina, S. Bhat, B.M. Wanklyn, and P.N. Kotru, *Mater. Chem. Phys.* 34, 257 (1993).
17. J.G. Bednorz and K.A. Muller, *Z. Phys. B Condens. Matter* 64, 189 (1986).
18. R. von Gelmont, J. Wecker, B. Holzphel, L. Schultz, and K. Samwe, *Phys. Rev. Lett.* 71, 2331 (1993).
19. B. Raveau, A. Maignan, and V.J. Caignaert, *Solid State Chem.* 117, 424 (1995).
20. R. Mahindiran, S.K. Tiwari, A.K. Raychaudhuri, T.V. Ramakrishnan, R. Mahesh, N. Rangavittal, and C.N. Rao, *Phys. Rev. B* 53, 3348 (1996).
21. J.B. Torrance, P. Lacorre, A.I. Nazzal, E.J. Ansaldo, and Ch. Niedermayer, *Phys. Rev. B* 45, 8209 (1992).
22. J.S. Zhou, J.B. Goodenough, and D. Dabrowski, *Phys. Rev. Lett.* 94, 226602 (2005).
23. X. Granados, J. Foncuberta, X. Obradors, and J.B. Torrance, *Phys. Rev. B* 46, 15683 (1992).
24. R. Kumar, R.J. Choudhary, M.W. Khan, J.P. Srivastava, C.W. Bao, H.M. Tsai, J.W. Chiou, K. Asokan, and W.F. Pong, *J. Appl. Phys.* 97, 093526 (2005).
25. R. Kumar, R.J. Choudhary, M. Ikram, D.K. Shukla, S. Molla, P. Thakur, K.H. Chae, B. Angadi, and W.K. Choi, *J. Appl. Phys.* 102, 073707 (2007).
26. S.A. Patil, Studies on physical properties of $Cu_xFe_{3-x}O4$ ferrites (Ph.D. thesis, Shivaji University, Kolhapur, 1981).
27. M.A. El Hitti, *J. Magn. Magn. Mater.* 164, 187 (1996).
28. M. Bhat, B. Kaur, R. Kumar, S.K. Khosa, K.K. Bamzai, P.N. Kotru, and B.M. Wanklyn, *Nucl. Instrum. Methods Phys. Res.* 245, 480 (2006).
29. D.G. Eorgiev, K.A. Krezhovt, and V.V. Nietv, *Solid State Commun.* 96, 535 (1995).
30. R.G.W. Brown, *J. Phys. E Sci. Instum.* 20, 1312 (1987).
31. S. Venugopalan, M. Dutta, A.K. Ramdas, and J.P. Remeika, *Phys. Rev. B* 31, 1490 (1985).

32. K. Manoj Singh, M. Hyun Jang, H.C. Gupta, and S. Ram Katiyar, *J. Raman Spectrosc.* 39, 842 (2008).
33. M.N. Iliev, M.V. Abrashev, H.G. Lee, V.N. Popov, Y.Y. Sun, C. Thomsen, R.L. Meng, and C.W. Chu, *Phys. Rev. B* 57, 2872 (1998).
34. H.C. Gupta, M.K. Singh, and L.M. Tiwari, *J. Raman Spectrosc.* 33, 67 (2002).
35. E. Traversa, P. Nunziante, L. Sangalatti, B. Allieri, and L. Depro, *J. Am. Ceram. Soc.* 83, 1087 (2000).
36. H. Guo, J. Burgess, E. Eda, S. Street, A. Gupta, M.N. Iliev, A.J. Kellock, C. Magen, M. Varela, and S.J. Pennycook, *Phys. Rev. B* 77, 172303 (2008).
37. S. Venugopalan and M.M. Becker, *J. Chem. Phys.* 93, 3833 (1990).
38. E. Anastassakis, A. Canterero, and M. Cardona, *Phys. Rev. B* 41, 7529 (1990).
39. I.H. Campbell and P.M. Fauchet, *Solid State Commun.* 58, 739 (1986).
40. R. Loudon, *Adv. Phys.* 13, 423 (1964).
41. H. Ritcher, Z.P. Wang, and L. Ley, *Solid State Commun.* 39, 625 (1981).
42. Y. Zhi and A. Chen, *J. Appl. Phys.* 91, 794 (2002).
43. K.K. Patankar, P.D. Dombale, V.L. Mathe, S.A. Patil, and R.N. Patil, *Mater. Sci. Eng. B* 8, 53 (2001).
44. J.C. Maxwell, *Electricity, Magnetism*, Vol. 828 (London: Oxford University Press, 1973).
45. K.W. Wagner, *Ann. Phys.* 40, 818 (1993).
46. C.G. Koops, *Phys. Rev.* 83, 121 (1951).
47. L.L. Hench and J.K. West, *Principles of Electronic Ceramics* (New York: Wiley, 1990), p. 189.
48. N.C. Tombs and J. Watkins, *Proc. Inst. Electr. Eng.* 104B, 145 (1957).
49. R.A. Waldron, *Ferrites: An Introduction for Microwave Engineers*, Vol. 40 (London: D. Van Nostrand, 1961).
50. E. Blechschmidt, *Phys. Z. Ver. Jahrb. Radioakt. Elektron.* 39, 212 (1938).
51. F.W. Brockman, P.H. Dowling, and W.G. Steneck, *Phys. Rev.* 77, 85 (1950).
52. G. Moltgen, *Z. Angew. Phys.* 4, 216 (1952).
53. L.L. Hench and J.K. West, *Principles of Electronic Ceramics* (New York: Wiley, 1990), pp. 202–206.
54. S.A. Lokare, R.S. Devan, and B.K. Chougule, *J. Alloys Compd.* 454, 471 (2008).
55. R.S. Devan, Y.D. Kolekar, and B.K. Chougule, *J. Alloys Compd.* 461, 678 (2008).
56. K.K. Patankar, S.S. Joshi, and B.K. Chougule, *Phys. Lett. A* 346, 337 (2005).
57. D. Adler and J. Feinleib, *Phys. Rev. B* 2, 3112 (1970).